ACADEMIC PRESS

Available online at www.sciencedirect.com
SCIENCE DIRECT®

Journal of Catalysis 218 (2003) 334–347

JOURNAL OF CATALYSIS

www.elsevier.com/locate/jcat

Nature and role of active states of Pd and Cu in the oxidative carbonylation of phenols with Pd/C and cuprous oxide

Won Bae Kim,[a] Eun Duck Park,[a] Chul Woo Lee,[b] and Jae Sung Lee [a,*]

[a] *Department of Chemical Engineering, Pohang University of Science and Technology (POSTECH), San 31, Hyoja-dong, Pohang 790-784, South Korea*
[b] *Department of Chemical Engineering, Hanbat National University, San 16-1, Dukmyung-dong, Yuseong-gu, Daejeon 305-719, South Korea*

Received 6 November 2002; revised 24 February 2003; accepted 5 March 2003

Abstract

Active states of palladium and copper for the oxidative carbonylation of phenol and bisphenol-A were investigated using X-ray absorption near-edge structure (XANES) and extended X-ray absorption fine structure (EXAFS) for Pd and Cu *K*-edges. The initial states of Pd and Cu were carbon-supported metallic Pd and cuprous oxide, respectively. During oxidative carbonylation, however, the metallic character of palladium was enhanced, as indicated by Pd *K*-edge XANES spectra taken before and after the reaction. Furthermore, Pd–Pd coordination number increased from ca. 6.0 to 11.0, as determined by the quantitative EXAFS analyses of Pd *K*-edge. The initial crystalline cuprous oxide was converted by reaction with Bu_4NBr into an unusual linear cuprous dibromide complex stabilized by tetrabutylammonium cation. Qualitative XANES and EXAFS analyses of Cu *K*-edge identified the structural and electronic configuration of the cuprous complex that was found to be the active main catalyst. There was a direct correlation between the formation of the cuprous complex and the catalytic activity and selectivity. Based on these results, a possible catalytic reaction scheme was proposed for the oxidative carbonylation of phenols with the catalytic system of Pd/C, an inorganic cuprous compound and Bu_4NBr.

Keywords: Active states; Pd metal; Linear cuprous dibromide complex; Role of Bu_4NBr; Oxidative carbonylation of phenols; XANES; EXAFS; Pd and Cu *K*-edges

1. Introduction

Oxidative carbonylation of phenol [1–12] or bisphenol-A (BPA) [13–15] has been studied to synthesize diphenyl carbonate (DPC) or polycarbonate (PC) oligomers, respectively. Both the DPC and the PC oligomers are key intermediates for PC synthesis without using the highly toxic and corrosive phosgene. These processes involving the direct oxidative carbonylations have a great advantage in that a fewer number of reaction steps are required from the raw material of CO to the final product of PC oligomers, compared with the current commercialized phosgene-free PC process that consists of many consecutive synthesis steps of carbonate intermediates such as dimethyl carbonate (DMC), DPC, and PC oligomers [16,17]. Recently, we found that a direct synthesis of phenyl carbonate-ended BPA oligomers in one-step was possible via a coupled oxidative carbonylation of BPA and phenol over the homogeneous Pd–Ce redox system [18] or the heterogeneous Pd/C with copper catalyst [19]. The coupled carbonylation was a simultaneous carbonylation of reactions (1) and (2) and a transesterification reaction (3) employing the same catalytic system in the same reactor. The selectivity of the proposed reaction for the desired *para*-positioned carbonylation was significantly affected by catalytic components, especially by the state and the structure of copper cocatalyst [19].

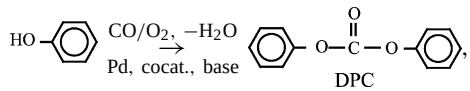

(1)

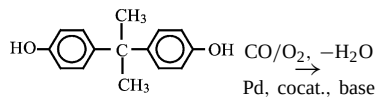

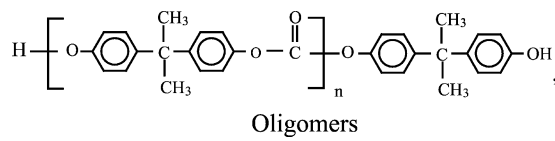

(2)

* Corresponding author.
E-mail address: jlee@postech.ac.kr (J.S. Lee).

0021-9517/03/$ – see front matter
doi:10.1016/S0021-9517(03)00089-7

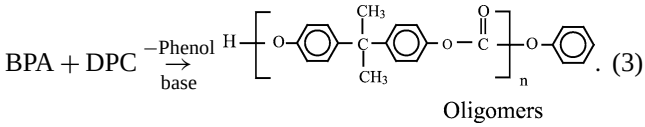

(3)

Most research on the oxidative carbonylation of phenols has been carried out employing Wacker-type redox pair catalysts of a homogeneous Pd complex and an inorganic metal salt among Cu, Ce, Co, or Mn compounds with a proper base such as tertiary amine or quarternary ammonium halide [1–6,13–15,18]. Following Wacker chemistry established for the oxidation of olefins or CO, the homogeneous Pd(II) complex is the main catalyst to coordinate phenoxides and CO in the oxidative carbonylation and gives an aromatic carbonate and Pd^0 by reductive elimination [1–6,13–15]. The reduced Pd^0 is then reoxidized to the active Pd^{2+} by reduction of the inorganic metal salt and/or organic cocatalysts such as benzoquinone. The reduced cocatalysts are subsequently reoxidized by molecular oxygen, completing the overall catalytic cycles.

To efficiently recover the used Pd catalysts after the liquid-phase reactions, there have been several recent studies on heterogeneous Pd catalysts such as carbon-supported metallic Pd (Pd/C) [7–12,19]. While the mechanistic consideration with the homogeneous system has been well established, studies of the nature and the role of active catalytic components and quarternary ammonium halide are rare for catalyst systems involving the heterogeneous Pd/C, due to the lack of appropriate characterization techniques and the difficulty in analyzing the used catalysts. As an attempt to understand the active states of Pd/C employed for the oxidative carbonylation catalyst, there was a report that Pd^{2+} leached from the metallic phase seemed to catalyze the reaction because a large amount of the soluble palladium was detected from the elemental analysis of liquid-phase reaction mixtures [7]. Thus the scheme involving the homogeneous Pd^{2+} species was essentially the same as the conventional homogeneous Pd-cocatalyst redox mechanism. However, the experimental evidence for this suggestion is far from convincing.

X-ray absorption fine structure (XAFS) appears to be most proper and direct method of investigating the active states of catalytic components in this reaction system because it is hardly affected by organic media of the reaction mixture and enables each metal of interest to be analyzed separately. In the present work, Pd/C and Cu remaining in the reaction mixture after the oxidative carbonylation are characterized by XAFS. As an initial copper precursor, we used Cu_2O that was found to be the most efficient partner with Pd/C in our previous screening experiments [19]. The structural and chemical information of Pd and Cu will be correlated with their catalytic activities. Also a mechanistic scheme will be proposed with possible roles of the catalytic components.

2. Experimental

2.1. Preparation of carbon-supported Pd

Pd-supported on activated carbon (denoted as Pd/AC, 1 to 20 wt% Pd loaded) was prepared by a wet impregnation method. Activated carbon (Aldrich; BET surface area of 1075 $m^2\,g^{-1}$), which was dried at 383 K for 12 h in an oven before impregnation, was mixed with a solution of $Pd(CH_3COO)_2$ dissolved in acetone. This slurry was dried in ambient air at 333 K for 1 h to remove the acetone and dried further under a reduced pressure of ca. 100 Torr in a rotary evaporator. The impregnated Pd acetate on the AC was then reduced into metallic Pd under a dihydrogen stream of 37 $\mu mol\,s^{-1}$ at temperatures of 473 to 973 K for 4 h in an U-type quartz reactor. All reagents except Cu_2O (Alfa) were purchased from Aldrich and were used as received.

2.2. Oxidative carbonylation of BPA and phenol

The 5 wt% Pd/AC (0.01 mmol of Pd), 0.1 mmol of Cu_2O, 0.5 mmol of 1,4-benzoquinone (BQ) as an organic cocatalyst, 0–1 mmol of tetrabutylammonium bromide (Bu_4NBr, TBAB), 30 cm^3 of tetrahydrofuran (THF) as a solvent, 10 mmol of BPA, and 20 mmol of phenol were charged into a 100-cm^3 autoclave (Parr). The 5 wt% Pd/AC was prereduced at 473 K. After purging the reactor with O_2 three times, 5 MPa of CO and 0.5 MPa of O_2 were charged successively and the reaction temperature was adjusted to 373 K. The reaction was quenched after 4 h of reaction time by cooling the reactor with ice water. Reaction products were analyzed by high-performance liquid chromatography (HPLC) using the reverse-phase method, together with gas chromatography (GC) and GC-mass spectrometry (GC/MS) in order to identify and quantify the desired products as well as by-products.

2.3. XAFS measurements and data analysis

XAFS measurements were conducted on the beamline 10B of the Photon Factory in the National Laboratory for High Energy Physics (KEK) in Tsukuba, Japan [20]. The spectra were taken at room temperature in a transmission mode for the *K*-edges of Pd and Cu. The intensity of X-ray was monitored using ionization chambers purged with a pure Ar gas for both the incident and the transmitted beams in the measurements of the Pd *K*-edge. For Cu *K*-edge measurements, the detector gases were N_2 (100%) for the incident beam and N_2 (85%) + Ar (15%) for the transmitted beam. As standard reference materials, XAFS data were obtained for Pd references such as Pd foil, $PdBr_2$, $Pd(CH_3COO)_2$, and PdO and for Cu references of Cu foil, Cu_2O, CuBr, CuO, and $CuBr_2$.

To observe the structure of Pd and Cu remaining in the reaction media and achieve an optimum X-ray transmission intensity for Pd *K*-edge, the product mixture containing

catalytic components and reagents after the reaction was filtered to reduce the total volume into one-third with a 0.45-μm PTFE polymer filter. The filtered catalyst-rich reaction sample was then evaporated to remove THF under a reduced pressure, resulting in a gel-like mixture consisting of the catalytic components, unreacted reagents, and oligomeric aromatic carbonate products. This sample preparation method allowed the optimum X-ray absorption for both Pd and Cu without disturbing their active states in the reaction media. Although it was conducted in ambient air, there was no effect by atmospheric dioxygen and water on the resulting Pd and Cu phases. XAFS spectra were obtained using a Kapton window sealed-Teflon tubing spacer with an outer diameter of 1/2 inch containing a gel-like mixture injected by microsyringe just before the measurement. The length of the Teflon tubing spacer was adjusted from 2 to 15 mm according to prior calculations for the optimum X-ray absorption.

The XANES function for both Pd and Cu compounds was analyzed with the WinXAS 97 program [21]. The background correction and the normalization of the spectrum were processed by a least-squares fit. The preedge background was removed through fitting a preedge region with a straight line and subtracting the extrapolated values from the entire spectrum. The resulting elemental absorption $\mu(E)$ was then normalized by using atomic-like absorption $\mu_0(E)$ at the edge that was calculated with a cubic spline fit in the postedge region.

The EXAFS data for both Pd and Cu compounds were analyzed using the UWXAFS 3.0 package [22] and the FEFF 7.0 code [23], both licensed from University of Washington. The preedge background was removed by using a simple line fitting. The interference function of the EXAFS data is defined as $\chi(E) = [\mu(E) - \mu_0(E)]/\Delta\mu_0(E_0)$ above the absorption edge (E_0), where $\mu(E)$ is the absorption coefficient due to the particular edge of the element of interest in the sample, $\mu_0(E)$ is the atomic-like absorption, and $\Delta\mu_0(E_0)$ is the jump at the edge step. The postedge background function $\mu_0(E)$ is approximated by a piecewise spline that can be adjusted so that low-R components of the Fourier-transformed data $[\chi(R)]$ are optimized. The power-scaled EXAFS function $k^n\chi(k)$ in the momentum k space was converted to the real space, i.e., R-space, by Fourier transformation, resulting in the radial structural function (RSF) of the sample. For Fourier transformation, $k_{\min}$ and $k_{\max}$ were chosen in the ranges of 1.4–2.8 and 11.6–12.8 Å^{-1}, respectively, for Pd EXAFS. For Cu, the k values in the ranges of 2–3 and 12–13 Å^{-1} were selected as $k_{\min}$ and $k_{\max}$, respectively. A Hanning window sill was used to reduce the truncation effect from the Fourier transformation over a finite range. The nonlinear EXAFS fitting was performed in R-space without Fourier filtering. The theoretical standard for Pd–Pd single scattering was synthesized with the FEFF code using structural information for Pd metal [24]. A single adjustable parameter in the XAFS analysis, the amplitude reduction factor S_0^2, was taken to be 0.81 for Pd, which was found by fitting the experimental RSF of Pd foil with the theoretical one.

3. Results

3.1. Effects of Bu_4NBr on the oxidative carbonylation of phenols with Pd/C and Cu_2O

Quarternary ammonium halides have been frequently used as bases in the oxidative carbonylation of phenols to generate phenoxides which readily make a nucleophilic attack on the main catalytic component [3–8]. These halide salts, especially Bu_4NBr (TBAB) and Bu_4PBr, show much better performance even with a smaller amount than that of a simple alkali base or Lewis base such as tertiary amines [18]. While its role as a base has been investigated in many studies, other effects as a surfactant [5], a phase transfer catalyst [3], and a halide source [3] were suggested but have not been well understood yet due to the lack of the mechanistic considerations of a catalytic system through appropriate characterization techniques.

Fig. 1 shows the effects of the amount of TBAB on the oxidative carbonylation of BPA and phenol, which is one of the most critical variables affecting the activity and the selectivity in the reaction. For convenience, the samples of the reaction mixtures after the reaction were denoted as S1, S2, S3, S4, S5, and S6 according to the ratios of TBAB/Pd with 0, 5, 10, 30, 50, and 100, respectively. As the TBAB/Pd ratio increases from 0 to 50 with the fixed amount of Pd (0.01 mmol), the reaction rates and the selectivity of the desired products increased with the same trend whereas the selectivity of by-products was reduced rapidly. Above the TBAB/Pd ratio of 50 (S5), the effect was saturated or seemed slightly deteriorating. The reaction rates were based on the conversion of BPA and the respective selectiv-

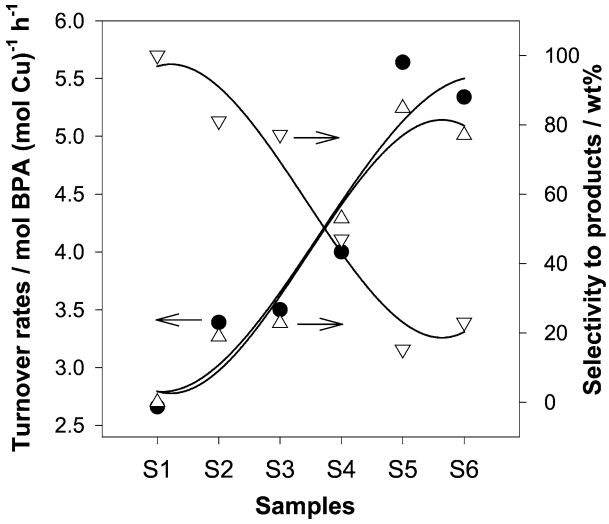

Fig. 1. Effects of the amounts of Bu_4NBr on the reaction rates (●) and the selectivities of p-positioned carbonylation products (△) and by-products (▽).

ities were defined as the desired *para*-position-carbonylated products or by-products among the products converted from BPA. The desired products consisted of dihydroxy-ended [from the reaction (2)] and monophenyl carbonate-ended oligomers [from reaction (3)], where the number of repeating units (n) of BPA carbonate was dominantly 1 and 2, and up to 5. By-products were *ortho*-position-carbonylated and isomerized products from BPA [18]. For the effect of TBAB amount in the catalytic system, an optimum value appeared to exist. As TBAB increases, the reaction becomes faster and more selective up to the optimum amount of 50 of TBAB/Pd ratio (S5), and then the reaction rate and the selectivity to the desired products seem to decrease above the amount. Based on the results of the catalytic activity and the product selectivity in Fig. 1, the active states of Pd and Cu and the roles of TBAB will be elucidated in our catalytic system through the following XAFS characterizations.

3.2. Pd *K*-edge XANES before and after the reaction

The XANES represents X-ray absorption accompanied by an electronic transition from inner level to outer unoccupied levels, which contains information on chemical environments of the X-ray absorbing atom and the nature of surrounding ligands or metals [25]. The Pd *K*-edge XANES spectra of reference compounds were investigated in Fig. 2. The absorbing Pd *K*-edge in each spectrum corresponds to the allowed $1s \rightarrow 5p$ transition, merging into the continuum at higher energies above the edge. Pd foil shows a distinctly different shape in the XANES compared to the other Pd reference compounds, as shown in the figure, which could be characterized by two strong peaks at ca. 24360 eV and ca. 24384 eV. $PdBr_2$ has no peak above the edge. Pd acetate and PdO show one broad peak at around 24365 and 24360 eV, respectively. The shape and peak position can be used in order to identify an unknown Pd XANES spectrum by comparison with known reference XANES spectra.

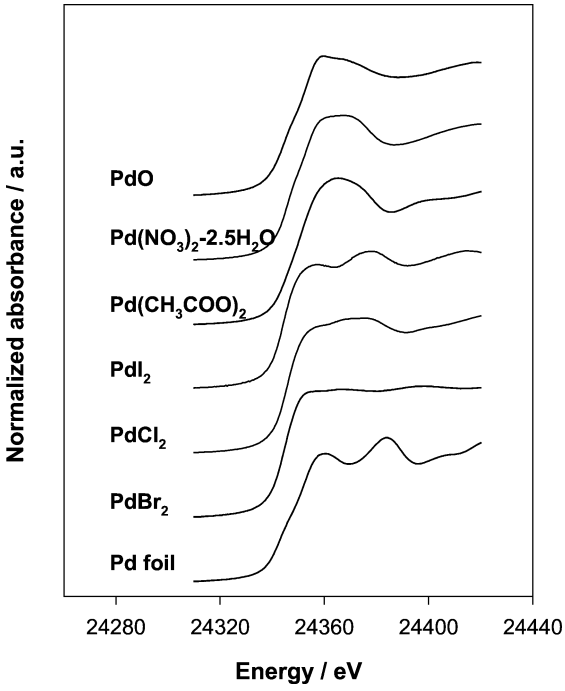

Fig. 2. Pd *K*-edge XANES spectra of the reference compounds.

Fig. 3 shows XANES spectra of the fresh 5 wt% Pd/AC catalysts reduced at 473 or 973 K and the used catalysts after the carbonylation with different amounts of TBAB. While the strong metallic character of Pd in 5 wt% Pd/AC was observed upon reduction at 973 K, the spectrum of the fresh 5 wt% Pd/AC reduced at 473 K did not show such a strong metallic character of Pd, as judged from the weak peaks at ca. 24360 and ca. 24384 eV that were present in the Pd foil spectrum. The XANES of 5 wt% Pd/AC reduced at 473 K represented a combined phase between the metallic and the oxidized Pd [19]. The latter might be originated from surface oxidation that occurred when the sample was exposed to the ambient air for 1 day as a passivation procedure of the Pd/AC catalysts after the reduction treatment. Considering that the 5 wt% Pd was impregnated on the support AC with a surface area of 1075 $m^2\,g^{-1}$ followed by reduction treatment at a relatively low temperature of 473 K, the Pd metal would be highly dispersed so that the surface Pd could be readily oxidized with the molecular oxygen in the ambient air into surface PdO layers even at room temperature.

For all samples (S1–S6) after the carbonylation reaction, the Pd *K*-edge XANES showed the quite clear and enhanced

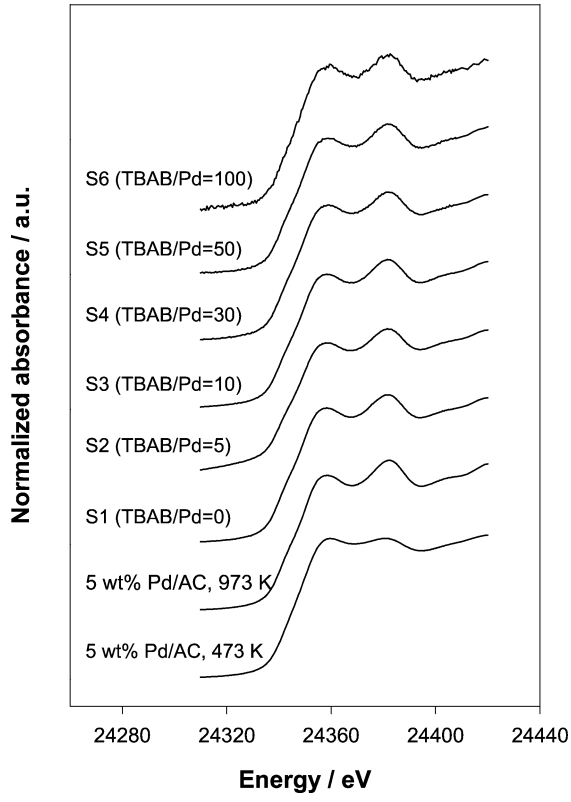

Fig. 3. Pd *K*-edge XANES spectra of the fresh and used catalysts after reaction with different TBAB/Pd ratios.

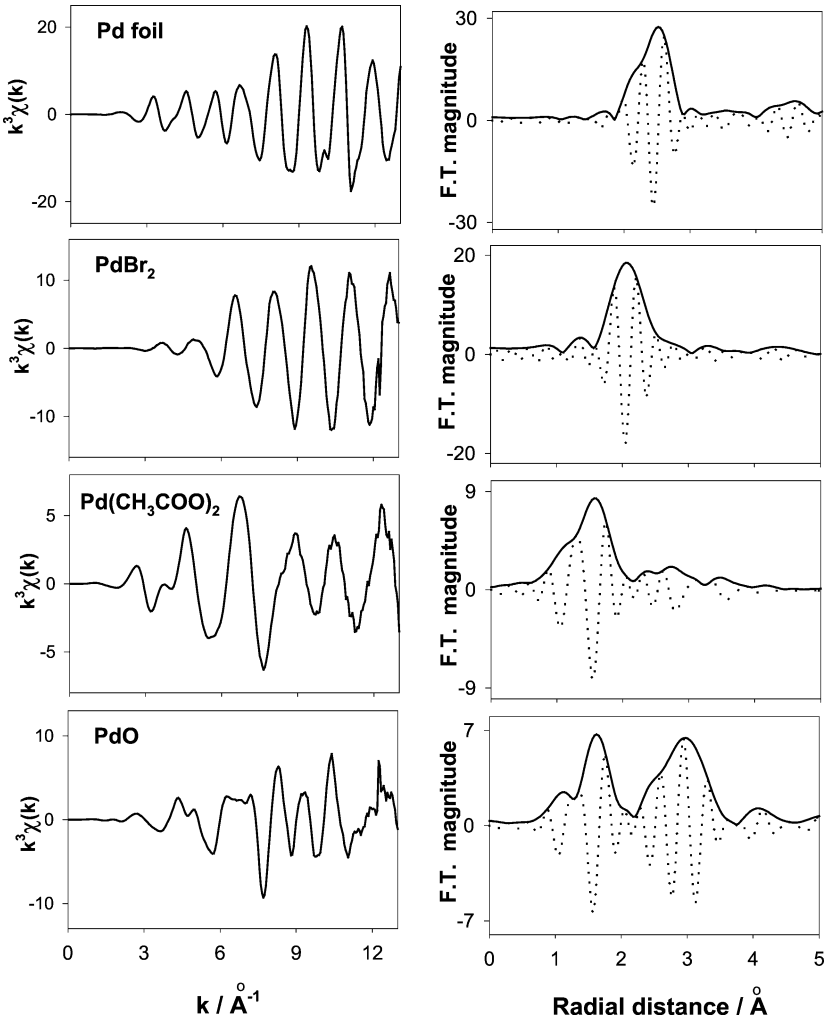

Fig. 4. k^3-Weighted EXAFS functions and their Fourier transformations about the Pd K-edge of some Pd reference compounds. The imaginary parts of the Fourier transformation are also plotted as dotted lines.

metallic palladium phase, compared with their initial state, namely, the fresh 5 wt% Pd/AC reduced at 473 K. The characteristic XANES peaks of Pd metal at ca. 24360 and ca. 24384 eV were strong enough to affirm that the palladium phase of the used catalysts after the reaction was a fully reduced metallic state similar to the reference Pd foil.

3.3. Pd K-edge EXAFS before and after the reaction

The EXAFS technique was adopted to characterize the structural states of palladium in the oxidative carbonylation of phenols. Small oscillations above the absorption edge in $\chi(E)$ can be extracted to produce EXAFS function $\chi(k)$ and its Fourier transformation gives the radial structural function. Major peaks in RSF correspond to important interatomic distances shifted from their true positions by a phase shift, and their intensities are closely related to the average coordination number of the atom at that distance. The Pd references in Fig. 4 show different oscillations in $\chi(k)$ and different phase-uncorrected distance peaks in their RSFs. In particular, the imaginary part of the Fourier transform clearly characterizes the nature of scatterers surrounding the palladium through a comparison of its shape and number of peaks. Based on these considerations, peaks at 2.5, 2.0, and 1.6 Å could be assigned to Pd–Pd, Pd–Br, and Pd–O interactions, respectively. Also the second shell of Pd–Pd interaction at 3.0 Å is shown in the RSF of the PdO reference.

The RSFs of some fresh Pd/AC catalysts are shown in Fig. 5 with different Pd loadings and reduction temperatures. Two important peaks were observed in the RSFs of 5 wt% Pd/AC reduced at 473 K. The peak at 1.6 Å appears only in the spectra of the sample of 5 wt% Pd/AC reduced at 473 K which is believed to come from Pd–O interactions as in the reference of PdO or Pd acetate. The other peak observed at 2.5 Å in all Pd/AC catalysts is evidently due to the Pd–Pd interaction of the metallic Pd. The former Pd–O interaction comes from the formation of Pd oxide, as seen from the previous XANES feature that represented the combined phase of both the metallic and the oxidized Pd, which could also be supported by our previous results regarding the effect of reduction temperature on the Pd structure of the fresh Pd/AC catalyst [19]. Note that the RSF of the refer-

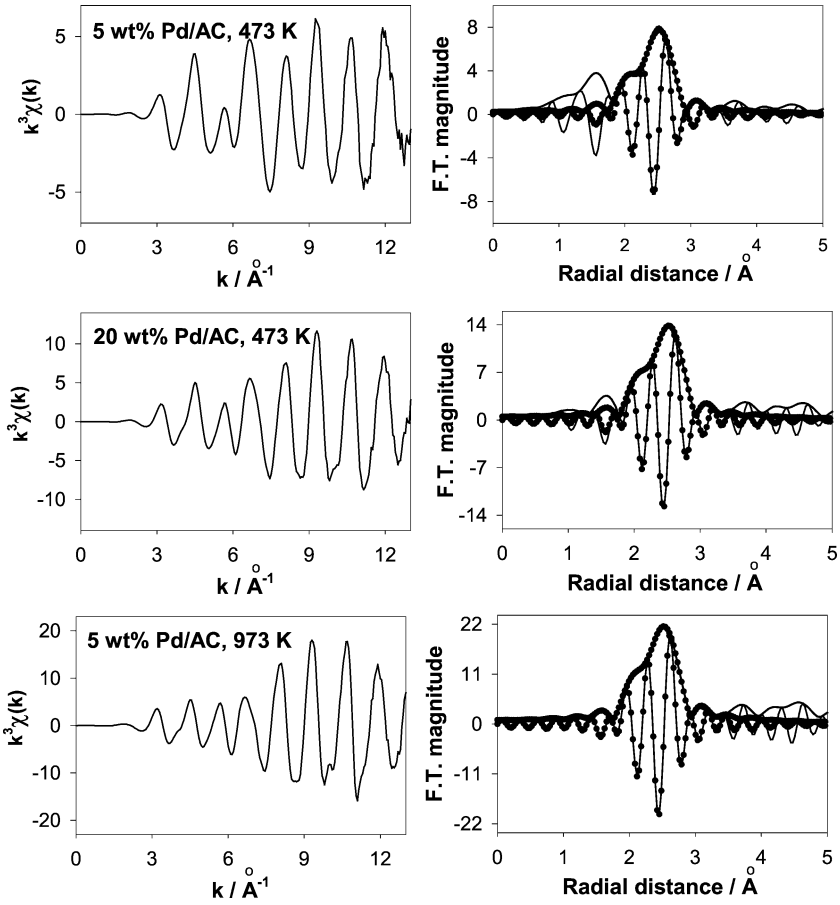

Fig. 5. k^3-Weighted EXAFS functions and their Fourier transformations about Pd K-edge of the fresh Pd/AC catalysts. The best fit results for the Pd–Pd interaction are also plotted as dots.

ence palladium oxide showed two peaks of Pd–O and Pd–Pd interactions with similar intensities. However, there is no or a very small second shell of the Pd–Pd peak at 3.0 Å in the catalyst sample of 5 wt% Pd/AC reduced at 473 K, suggesting that the Pd–O is present only on the surface, not in the form of three-dimensional bulk palladium oxide. Whereas the Pd–O interaction decreased as Pd loadings or reduction temperatures increased, the Pd–Pd peak drastically increased in its intensity, indicating that the particle size of the metallic Pd became larger.

Fig. 6 shows the RSFs obtained from Fourier transformation of the Pd K-edge EXAFS functions weighted with k^3 for the used catalysts after the reaction. The intensities of the Pd–Pd interaction peak at 2.5 Å were invariant with the amount of TBAB. However, the magnitudes of the peak were definitely all bigger than any of the fresh Pd/AC catalysts tested except the one reduced at 973 K. The EXAFS functions weighted with k^3 and their RSFs for the fresh Pd/AC catalysts and the used samples with the different TBAB/Pd ratios were shown together with their best-fitted function in dots. The quantitative information for the coordination number N and the radial distance R obtained by these EXAFS fittings is listed in Table 1 together with the Debye–Waller factor and the result of error analysis. The radial distances

Table 1
Pd K-edge EXAFS curve-fitting results for Pd/AC catalysts before and after the reaction

Sample	Shell	N	R (Å)	σ^2 [e] (Å^2)	R factor[f]
Pd foil[a]	Pd	12.0	2.751	–	–
5 wt% Pd/AC[b]	Pd	5.7	2.736	0.0079	0.0118
20 wt% Pd/AC[b]	Pd	8.0	2.741	0.0062	0.0016
573 K[c]	Pd	8.0	2.733	0.0073	0.0029
973 K[c]	Pd	10.9	2.741	0.0053	0.0009
S1 (TBAB/Pd = 0)[d]	Pd	11.1	2.742	0.0068	0.0025
S3 (TBAB/Pd = 10)[d]	Pd	10.1	2.742	0.0062	0.0002
S5 (TBAB/Pd = 50)[d]	Pd	11.2	2.736	0.0064	0.0048

[a] Theoretical model in the *fcc* phase of Pd metal.
[b] The fresh Pd/AC catalyst reduced at 473 K.
[c] The fresh 5 wt% Pd/AC catalyst reduced at these temperatures.
[d] The used Pd/AC catalyst after the reaction with different TBAB/Pd ratios.
[e] Debye–Waller factor.
[f] R factor gives a sum-of-squares of the fractional misfit, which is defined as $\sum_{i=1}^{N}\{[\mathrm{Re}(f_i)]^2 + [\mathrm{Im}(f_i)]^2\}/\sum_{i=1}^{N}\{[\mathrm{Re}(\tilde{\chi}_{\mathrm{data}\,i})]^2 + [\mathrm{Im}(\tilde{\chi}_{\mathrm{data}\,i})]^2\}$.

of the Pd–Pd seemed to be invariant in all cases, which were consistent with the value of Pd foil. However, the coordination number of the Pd–Pd of the fresh catalysts (5 wt% Pd loaded and reduced at 473 K) increased from 5.7 to 8.0

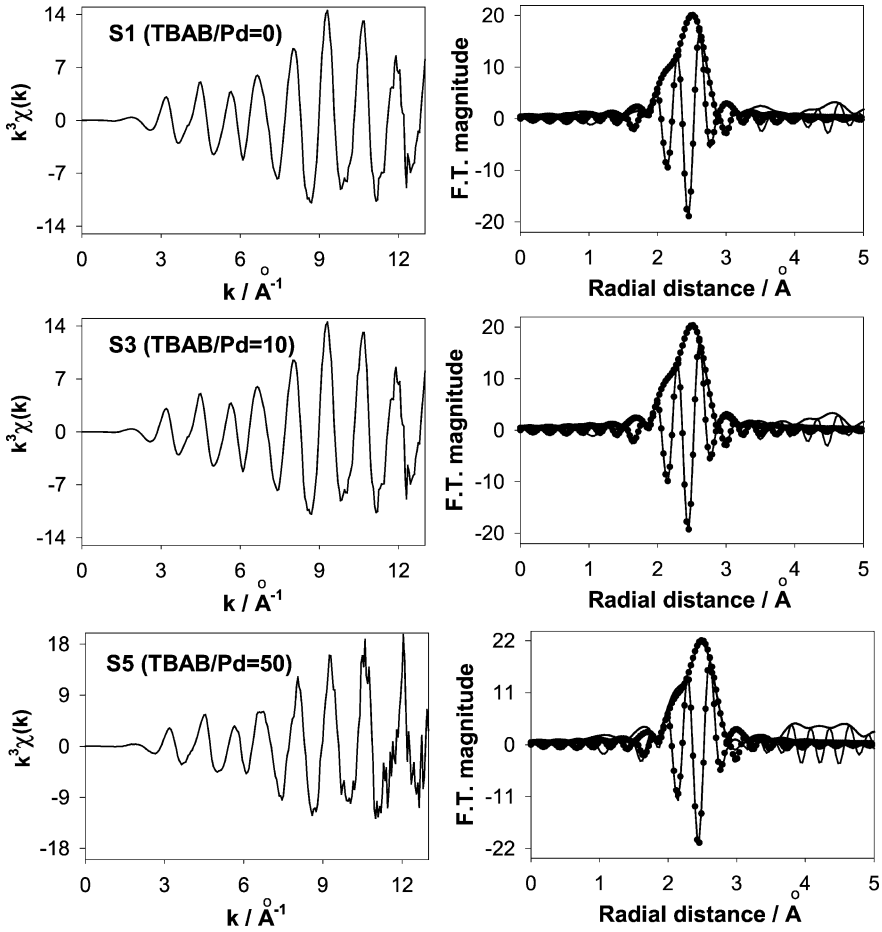

Fig. 6. k^3-Weighted EXAFS functions and their Fourier transformations about the Pd K-edge of some used catalysts with different TBAB/Pd ratios (reduced at 473 K) after the reaction at 373 K. The best fit results for the Pd–Pd interaction are also plotted as dots.

or to 10.9, with the increased Pd loading (up to 20 wt%) or the raised reduction temperature (up to 973 K), respectively. More importantly, the Pd–O peak disappeared and the Pd–Pd coordination number increased from 5.7 to 10–11 through the oxidative carbonylation reaction. This indicates clearly the enhancement of the metallic character of Pd from the combined state of PdO and Pd metal into the fully reduced metallic Pd with increased particle size of Pd after the reaction. The relative amount of TBAB to Pd did not give any apparent effect on the state of Pd after the reaction because the XANES and EXAFS spectra of S1–S6 did not show any significant difference irrespective of the amounts of TBAB introduced into the reaction system.

3.4. Cu K-edge XANES before and after the reaction

Fig. 7 shows XANES spectra of the copper references such as Cu foil, Cu_2O, CuBr, and CuO. The absorption edge of Cu K-edge XANES is assigned to the allowed $1s \rightarrow 4p$ transition. While Cu(0) and Cu(I) compounds have no hole in $3d$ orbitals, Cu(II) compounds are in a d^9 configuration. Therefore, a weak preedge peak representing the quadruple allowed $1s \rightarrow 3d$ transition appears below the edge in most Cu(II) compounds. A very weak but evident presence

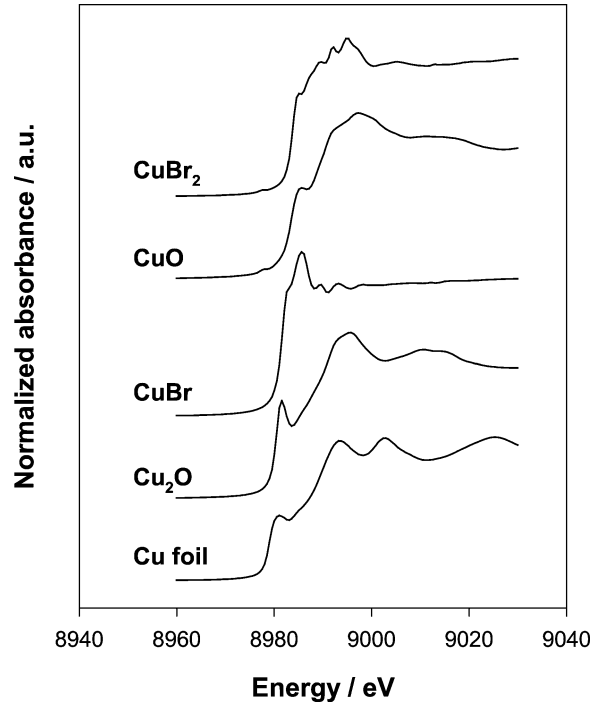

Fig. 7. Cu K-edge XANES spectra of the reference compounds.

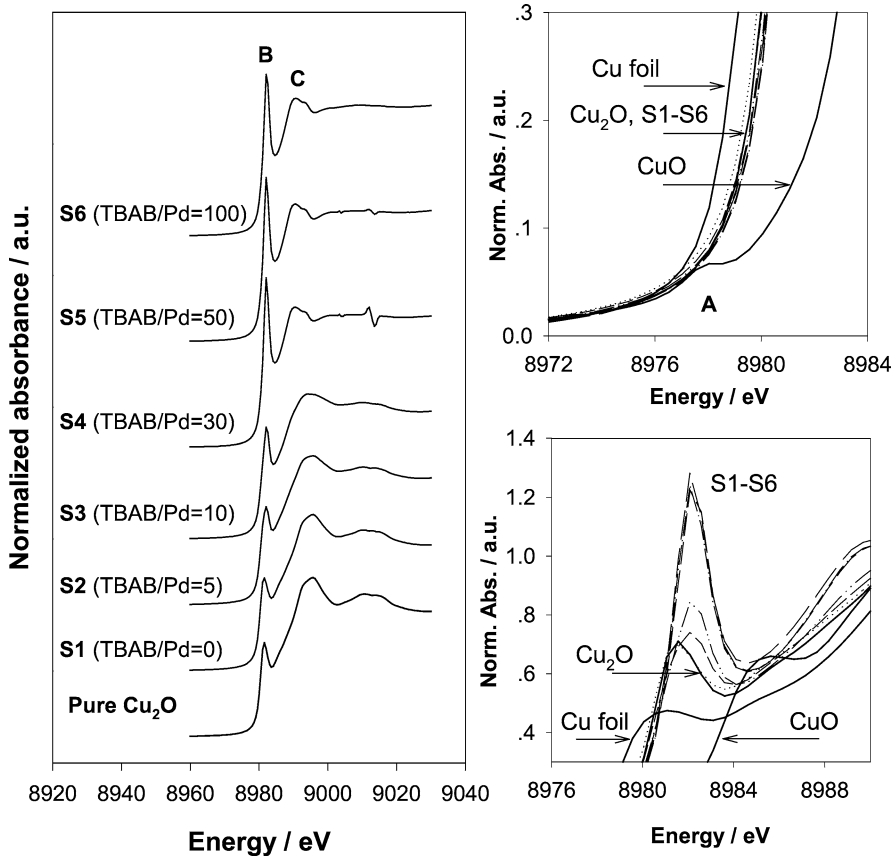

Fig. 8. Cu K-edge XANES spectra of the used catalysts after the reaction with different TBAB/Pd ratios.

of the preedge peak could be seen from the first and second derivatives of Cu(II) K-edge XANES spectra around 8976–8978 eV. This peak serves as a signature for a divalent copper, like the peak A in CuO in Fig. 8. The edge positions are also used to determine the oxidation state of Cu compounds, which reflect shifts to a higher energy as the oxidation number increases. The edge positions for the Cu references, which are defined as the energy that shows the maximum in the first derivative function of the rapidly rising edge step of the absorbance vs energy plot, were determined to be 8979.0, 8980.6, 8981.6, 8983.6, and 8983.8 eV for Cu foil, Cu_2O, CuBr, CuO, and $CuBr_2$, respectively.

Cu K-edge XANES spectra of the used catalysts after the reaction (S1–S6) were investigated as presented in Fig. 8. While the preedge peak A, which is shown in the right upper figure of the Fig. 8, corresponds to $1s \rightarrow 3d$ transition as explained previously, the peaks B and C as indicated in the left figure are usually assigned to $1s \rightarrow 4p$ transitions [26–28]. As the TBAB/Pd molar ratio increased, their XANES spectra were changed in shape as well as in peak intensity, especially of the peak B around 8980–8984 eV. The spectra for S1 and S2 showed almost the same shape as that of pure Cu_2O, but the XANES spectra evolved into completely different ones as the TBAB/Pd ratio increased from 10 to 100. The species responsible for these spectra were all in monovalent state of Cu(I) because they showed the edge energies in the range corresponding to Cu(I) compounds and had no preedge peak (the peak A) characteristic of Cu(II). Unfortunately, none of the Cu reference XANES spectra obtained here matched those of the samples with the higher TBAB/Pd such as S6. Therefore, it could be concluded that an unknown Cu(I) compound was formed when a large amount of TBAB was introduced in the reaction system.

3.5. Cu K-edge EXAFS before and after the reaction

k^2-Weighted EXAFS functions and their Fourier transformations for some Cu reference compounds are shown in Fig. 9. Copper references have different modes of oscillation in the $k^2\chi(k)$ and the different phase-uncorrected distance peaks in the RSFs. The imaginary parts of the Fourier transforms clearly characterize the nature of the scatterer surrounding copper by comparing their shapes and the number of peaks. From these considerations, the RSF peak at 2.2 Å represents the Cu–Cu interaction in Cu foil and those at 1.44 and 2.67 Å in Cu_2O are derived from Cu–O and Cu–Cu interactions, respectively. CuBr shows one radial distance of the Cu–Br interaction at 2.10 Å because the Cu in the reference of cuprous bromide has a tetrahedral symmetry and is surrounded by four Br anions.

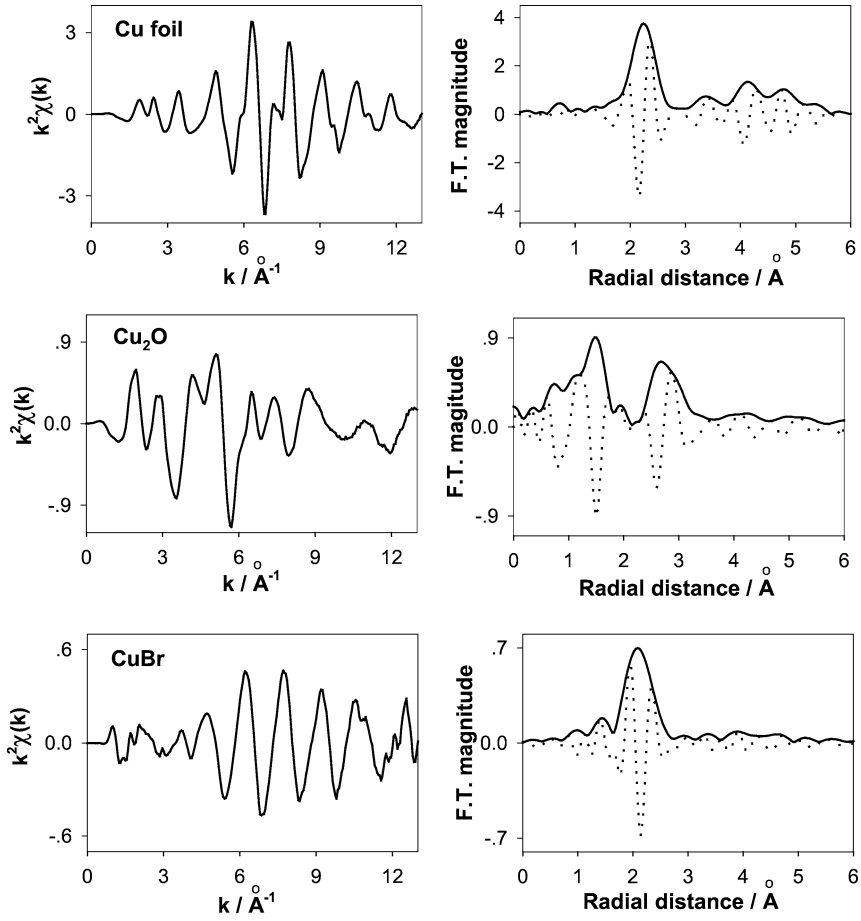

Fig. 9. k^2-Weighted EXAFS functions and their Fourier transformations about the Cu K-edge of some of the Cu reference compounds. The imaginary parts of the Fourier transforms are also plotted as dotted lines.

Fig. 10 shows the Fourier transforms of Cu K-edge EXAFS functions for the used catalysts after the reaction. As TBAB/Pd increases, the Cu–O and Cu–Cu interactions in Cu_2O structure disappear and a new single interaction of Cu-unknown ligand at 1.90 ± 0.03 Å appears. The RSF of the unknown Cu compound seems quite similar to that of the reference CuBr in terms of the shape of the RSF peak as well as the imaginary parts. However, it is definitely not the same structure of the crystalline reference CuBr because the unknown Cu(I) complex of S5 showed a completely different XANES shape from that of the reference CuBr and the RSF peak distance was shifted to a shorter distance by ca. 0.2 Å in S5 and S6. The unknown Cu(I) compound formed after the reaction is a monovalent Cu complex which might be coordinated with a ligand derived from TBAB because its formation was directly affected by the relative amount of TBAB to Cu_2O, as confirmed in the previous Cu K-edge XANES results. As an efficient base, TBAB was initially introduced in the oxidative carbonylation reaction system with an aim to activate phenols. However, the TBAB might play an additional role in converting the crystalline cuprous oxide into an unknown Cu(I)-TBAB complex.

4. Discussion

The oxidative carbonylation of BPA and phenol with the catalytic system of 5 wt% Pd/AC–Cu_2O–BQ–TBAB–THF showed unexpected but interesting features in the structures of Pd and Cu. The Pd state on AC showed an enhanced metallic character together with an increase in particle size, irrespective of the presence or the absence of TBAB. Apparently, the final state of Pd supported on AC after the reaction was not affected by the amount of TBAB either. However, the crystalline Cu_2O was converted to an unknown cuprous complex, whose formation depended on the amount of TBAB. This change in the state of copper was directly correlated with the catalytic reaction rates and the selectivity to the desired *para*-position-carbonylated bisphenol-A, as shown in Fig. 1, and could be monitored by Cu K-edge XANES and EXAFS.

4.1. Active states of Pd in the reaction

The Pd structures of Pd/AC catalysts were changed after the reaction. The fresh 5 wt% Pd/AC catalyst showed two weak but evident peaks above the edge of XANES spectrum,

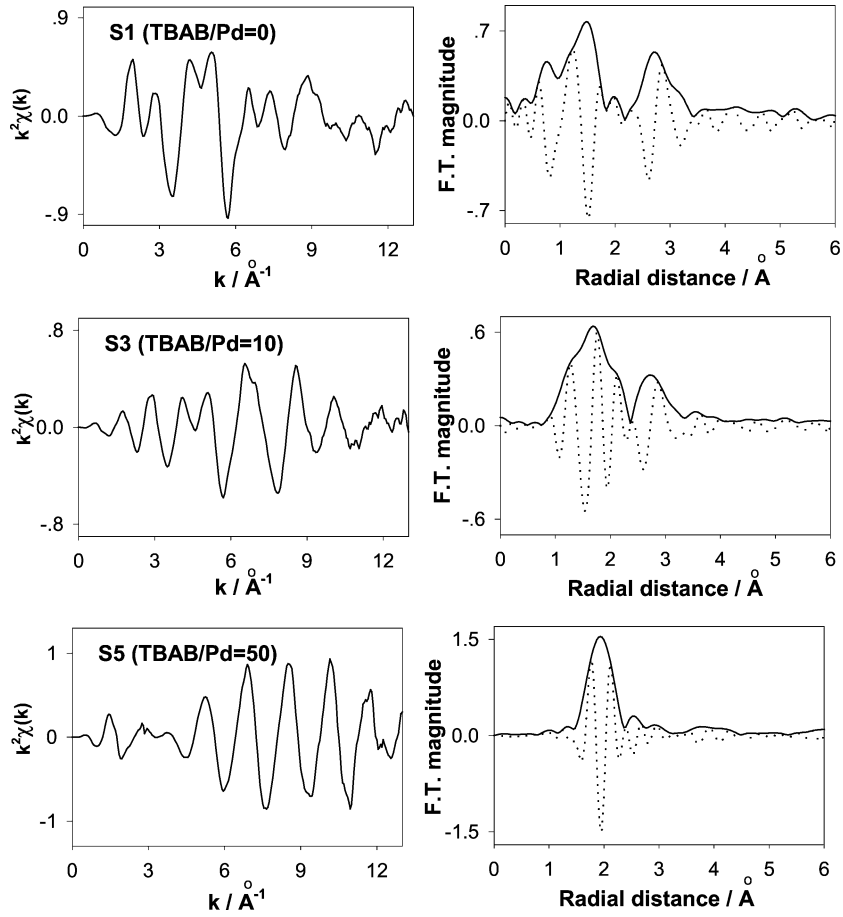

Fig. 10. k^2-Weighted EXAFS functions and their Fourier transformations about the Cu K-edge of some used catalysts after the reaction with TBAB/Pd ratios. The imaginary parts of the Fourier transformation are also plotted as dotted lines.

which corresponded to the metallic palladium. However, the $k^3\chi(k)$ EXAFS function of the 5 wt% Pd/AC revealed a slightly perturbed oscillation in the low k region, resulting in the Pd–O interaction at 1.6 Å as shown in its RSF. The Pd–Pd coordination number of the fresh catalyst was determined to be 5.7 from the Pd–Pd single-scattering curve fitting. For the used Pd catalyst after the reaction, however, all of XANES, $k^3\chi(k)$ EXAFS, and RSF indicated the completely metallic palladium phase which had increased coordination numbers (up to 11.2) of the Pd–Pd interaction. At the same time, Pd–O bonding disappeared after the reaction. In our previous work [19], variations in the initial Pd particle size by different Pd loadings or reduction temperatures gave a negligible effect on the reaction rates and the selectivity to the desired *para*-position-carbonylated products. Furthermore, the better performance was observed for the heterogeneous Pd/AC than for the best homogeneous Pd acetate catalyst tested under the same reaction conditions [19]. All the fresh Pd/AC catalysts converged to the fully reduced metallic Pd with enlarged sizes under the present conditions through the reaction, as shown in the Pd K-edge XANES and EXAFS. Therefore, the catalytic performance is independent of the initial states of Pd metallic character on activated carbon.

The increases in metallic character and size of Pd on AC might be explained by dissolution of some specific Pd through formations of molecular Pd complexes with tertiary amines [29] or with strong acids [30]. The Pd complexes would be redeposited rapidly on the surface of the supported metallic Pd under the present system because there is no sufficient stabilizer for the dissolved Pd species such as acids or phosphine ligands [30]. Also colloidal formation [31,32] of Pd particles might be involved in the redeposition of the dissolved Pd species in the presence of CO or protons with solvent of tetrahydrofuran or toluene [32]. When an excess amount of halide anions was present in our reaction system, we observed that the metallic Pd supported on AC was dissolved mostly to form Pd^{2+} species and existed stably in the reaction media after the reaction. With cupric dibromide or dichloride as Cu precursor instead of Cu_2O, the cupric compound was converted by Bu_4NBr into cuprous complexes to similar S5 and S6 as evidenced by the Cu K-edge XANES and most metallic Pd on the AC was dissolved to form Pd(II)Br_2 from the Pd K-edge XANES. Dissolution of the supported metallic Pd seemed to depend on the critical amount of halide anions that are able to ligate Pd and stabilize the Pd(II) complex. However, these catalytic systems resulted in poor catalytic activity and selectivity for the

desired products [19], suggesting that the dissolved molecular Pd^{2+} species did not provide good catalytic sites in the present reaction system.

Then, what is the role of the metallic Pd in this oxidative carbonylation condition? Is it still the main catalyst to interact with phenols and CO and transform them to the desired products? In the most conventional studies of the oxidative carbonylation of phenols employing the homogeneous Pd catalysts, it has been generally reported that the homogeneous Pd^{2+} catalyzes the reaction as the main component and is reduced to isolated Pd^0 species, which is in turn reoxidized by organic and inorganic cocatalysts such as benzoquinone or Cu^{2+}, respectively. However, this Wacker-type chemistry of Pd seems not to be involved in the present reaction scheme employing the Pd/AC because there was no soluble Pd species detected by ICP analysis (detection limit of ca. 1 ppm) that might be leached from the Pd/AC. The authentic homogeneous $Pd(CH_3COO)_2$ catalyst showed far inferior activity to the Pd/AC. Furthermore, the catalytic activity and the selectivities to the products depended directly on the formation of the Cu(I) complex transformed from Cu_2O and TBAB, as shown in Fig. 1 and the previous Cu *K*-edge XANES results. Finally, the carbonylation reaction proceeded readily even with only Cu_2O without any Pd source, resulting in substantial formation of the desired *para*-position carbonylation products, but there was no reaction occurring over Pd/AC itself when a cuprous catalyst was absent under the present reaction conditions [19]. Therefore, the metallic Pd under the present reaction conditions does not seem to be the main catalyst, but may play a different role.

4.2. Identification of a linear cuprous dibromide complex

Cu(I) compounds have important functions in some life processes, e.g., metalloproteins, representing neutral, anionic, or cationic complexes with Cu(I)–ligand bonds [26]. The highest coordination number of Cu(I) is 4, but 2 and 3 are also present [33,34]. A few Cu(I) species reveal a characteristic peak at 8980–8985 eV like the peak B in Fig. 8, whose feature is sensitive to the central Cu's geometric environment [26,33,34]. The high intensity of the peak is consistent with the allowed electric dipole transitions of $1s \rightarrow 4p$ and $1s \rightarrow$ ligand group orbitals, since electric quadrupolar transitions are considerably weaker [33]. The intensity of the peak increases as the coordination number of Cu(I)–ligand decreases from 4 to 2 or the coordination symmetry decreases [26,33]. Therefore, the characteristic peak B in the Cu(I) *K*-edge XANES can be used as a direct indicator for the coordination number and the geometric environment. Thus, a very intense and narrow peak B indicates that the structure of Cu(I) is two coordinated with ligands and has a linear arrangement [26–28,33–36].

Kau et al. [26] studied extensively and summarized the representative amplitudes and the energy positions of the Cu *K*-edge XANES peaks for various Cu(I) and Cu(II) compounds, based on the measurements of 19 Cu(I) and 40 Cu(II) model complexes. They systematically correlated the Cu *K*-edge XANES features with the oxidation states and the geometric structures. In particular, the energy position and the normalized intensity of the peak B at 8980–8984 eV were compared with the number of ligands and the site geometry of the Cu(I) complexes. The splitting peaks in the region of the rapidly rising edge like peaks B and C in Fig. 8 could be observed in the cuprous compounds having the linear configuration with two ligands. This phenomena could be explained by the ligand field splitting of Cu $4p$ orbitals because peak B corresponds to the degenerate $1s \rightarrow 4p_{x,y}$ transition and peak C represents $1s \rightarrow 4p_z$ transition as described elsewhere [26,28]. For a linear Cu(I) with two coordinated ligands, a repulsive interaction of the ligand field along the z axis resulted in raising the energy of the antibonding copper $4p_z$ molecular orbitals relative to the $4p_{x,y}$ levels [26,28]. Thus, the transition from $1s$ to the doubly degenerated $4p_{x,y}$ final state would result in an intense peak at a lower energy than the peak due to the $1s \rightarrow 4p_z$ transition [26].

The normalized intensity of peak B for our samples S4–S6 is in the range of 1.2–1.3 as shown in Fig. 8. These values are slightly higher but close to the normalized intensities (0.9–1.1) for the two-coordinated linear Cu(I) compounds reported by Kau et al. [26]. The peak B energy positions, which were calibrated by the edge energy of Cu metal to correct the energy scale, also suggest that the copper in S4–S6 has a linear geometry configuration with two ligands. The ligand appears to be bromide anion derived from Bu_4NBr because the imaginary parts in RSF, which characterize the nature of backscatterer [37], show the shape and the number of oscillations similar to those of the Cu–Br interaction in the reference CuBr, although the phases are slightly shifted as shown in Fig. 11. The shift by ca. 0.2 Å in the phases of EXAFS function can be attributed to the difference in structural configurations between the reference CuBr and our sample of S6. The slight difference of the frequency in $k^2\chi(k)$ functions may come from the difference in the radial distance [37].

A Cu(I) complex was also reported with the XANES features strikingly similar to those of our samples S4–S6. Rothe et al. [28] observed a monovalent Cu in the linear 2-fold coordination with Br anions as an intermediate during the preparation of N(octyl)$_4$-stabilized metallic Cu colloid through reducing $[N(octyl)_4]_2[CuCl_2Br_2]$ complexes by $Li[BEt_3H]$ in toluene. The XANES spectrum of the proposed linear $[Br^-–Cu(I)–Br^-]^-$ complex was very similar to our XANES spectrum in terms of the normalized intensities, the energy positions of peaks B and C, and the overall shape. Thus, our S4–S6 samples contain essentially the same type of Cu(I) complex. Since the complex needs a countercation to compensate for its negative (-1) charge, Bu_4N^+ should be available to stabilize the linear cuprous dibromide species by an electrostatic interaction. In summary, the Cu(I) complex in S4–S6 seems to be $[Br^-–Cu(I)–Br^-]^-\cdots{}^+NBu_4$

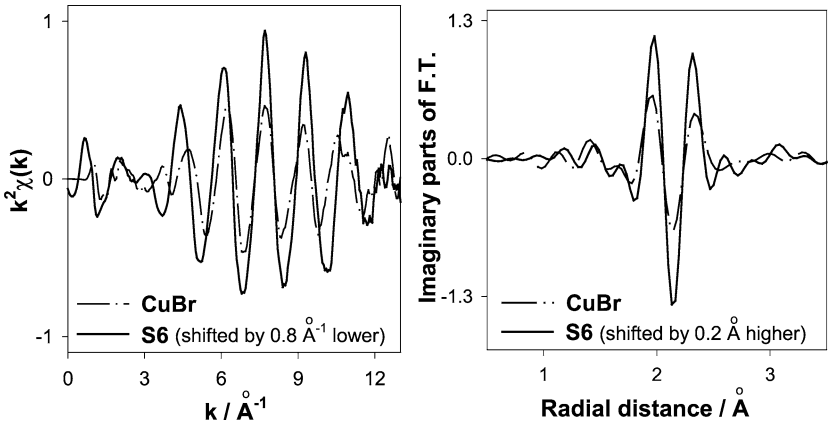

Fig. 11. Comparison of EXAFS functions between the reference CuBr and the sample S6.

(denoted as cuprous dibromide complex or CDC) that is formed in our reaction system during the oxidative carbonylation of BPA and phenol.

4.3. Reaction scheme of oxidative carbonylation of BPA and phenol

Fig. 12 illustrates a schematic of the CDC formation from Cu_2O with TBAB and shows the possible molecular configuration of the CDC. The bromide anion in TBAB attacks the central Cu(I) in Cu_2O and replaces oxygens by breaking the Cu–O bonds. Since the 2-fold coordinated $Cu(I)Br_2$ species is in one electron negative charge, this species interacts with the tetrabutylammonium cation to compensate for the charge distribution. Because the Cu complex should have only two ligands as inferred from its characteristic XANES feature, this cation should not directly coordinate to Cu, but could be connected by the electrostatic interaction between the two different ionic compounds. Therefore, the CDC has configuration in which Cu(I) has two ligands of bromide anions in a linear arrangement and the ammonium cation plays roles of compensating for the charge and stabilizing the linear $[Cu(I)Br_2]^-$ complex. The complete transformation of cuprous oxide by TBAB into the CDC was attained for S4–S5 as judged from the Cu *K*-edge XANES and EXAFS analysis, which could be also predicted from the stoichiometric amount of TBAB relative to the cuprous oxide (4 mol/1 mol).

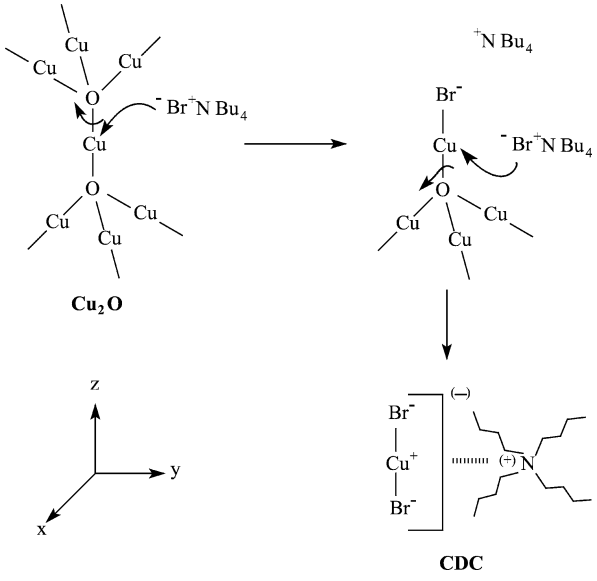

Fig. 12. A proposed reaction scheme for the formation of the linear cuprous dibromide complex (CDC) from Cu_2O and Bu_4NBr.

In Scheme 1, we propose a catalytic reaction scheme based on the proposed active states of catalysts for the oxidative carbonylation of phenols. As an initiation step, the CDC coordinates phenol or BPA denoted as ArOH. A CO molecule is inserted into complex **I** to form complex **II**, followed by reductive elimination from the two complexes like reaction (5) or a direct reaction of ArOH with the complex **II**, resulting in the production of aromatic carbonates with coproduction of Cu(0) and TBAB molecules. The reduced and isolated Cu^0, which should be short lived, is reoxidized by BQ in the presence of acid (HBr) through the formation of a metal–BQ complex [38] and simultaneously returns to its initial active state of the CDC. This reoxidation of Cu^0 to

$$\underset{\textbf{CDC}}{(BrCuBr)(NBu_4)} + ArOH \xrightarrow{HBr} \underset{\textbf{I}}{(BrCuOAr)(NBu_4)} \xrightarrow{CO} \underset{\textbf{II}}{(BrCu\overset{O}{\overset{\|}{C}}OAr)(NBu_4)}, \tag{4}$$

$$\textbf{I} + \textbf{II} \rightarrow (ArO\overset{O}{\overset{\|}{C}}OAr) + 2Cu^0 + Bu_4NBr, \tag{5}$$

$$2Cu^0 + 2HBr + BQ \rightarrow 2Cu^+ + 2Br^- + HQ, \tag{6}$$

$$Cu^+ + Br^- + Bu_4NBr \rightarrow \textbf{CDC}, \tag{7}$$

$$HQ + \tfrac{1}{2}O_2 \xrightarrow[Pd/AC]{} BQ + H_2O. \tag{8}$$

Scheme 1. A proposed reaction scheme based on the catalytic cycle with the CDC as the main active catalytic species for the oxidative carbonylation of phenols using the catalyst system of Pd/AC–Cu_2O–BQ–TBAB.

Cu^+ could be evidenced by a ready oxidation of bulk Cu metal to the cuprous complex under the present reaction conditions. We observed that XANES spectra very similar to those of S4–S6 appeared after the reaction when copper metal was used as the initial Cu precursor instead of Cu_2O under the same reaction conditions. This means that the metallic copper can be readily converted to the cuprous complex CDC. Also we tested reaction step (6) itself in order to investigate the feasibility of reduction of BQ to HQ under the following conditions: the amount of copper metal powder = 10 mmol; the initial amount of BQ = 5 mmol; the amount of HBr = 10 mmol; the amount of THF = 30 ml; the initial pressure of N_2 = 0.5 MPa; the reaction temperature = 373 K; the reaction time = 4 h. After mixing the reactants and the solvent, we found that ca. 60% of the initial BQ was converted to HQ even at room temperature just before the reaction started, suggesting that this reaction is very fast and readily occurs. Using this mixture of 2 mmol of BQ and 3 mmol of HQ, further conversion of BQ was achieved up to 90% after the reaction for 4 h at 373 K. The final compositions were 0.5 mmol of BQ, 4.15 mmol of HQ, and others of unknown by-products. The Cu^{2+} species may not be involved in the present catalytic cycle, as we have not seen any trace of its presence in our present reaction system.

The Pd/AC is supposed to catalyze the formation of the sole by-product H_2O through reaction (8) between molecular oxygen added externally and two protons in hydroquinone (HQ). This step regenerates BQ to be used in the step (6). In order to make clear the role of metallic Pd supported on activated carbon, this reaction step (8) was also tested under the following condition: the amount of 5 wt% Pd/AC (the same catalyst used in our work) = 0.213 g (0.1 mmol of Pd); the initial amount of hydroquinone (HQ) = 5 mmol; the amount of THF = 30 ml; the initial pressure of O_2 = 0.5 MPa; the reaction temperature = 373 K; the reaction time = 4 h. After the reaction, we observed that 4.6 mmol of HQ was converted to benzoquinone with a selectivity of 97% or higher by gas chromatography, which corresponded to 95% of HQ conversion and 92% of BQ yield. Without the Pd/AC catalyst under this condition, the conversion of HQ was achieved to less than 40% (ca. 38%). Therefore, it could be concluded that the supported metallic Pd catalyst serves as an excellent catalyst for the regeneration of BQ from HQ in our reaction condition.

The coordination of phenols to the CDC is expected to be the rate-determining step due to the steric hindrance caused by the bulk tetrabutylammonium cation. However, the formation of complexes **I** and **II** and the reductive elimination of those would proceed rapidly because of the low stability of the species, considering their steric and electronic unbalances. The proposed reaction scheme shows that the oxidative carbonylation of phenols with the Pd/AC and Cu_2O proceeds in a completely different manner from the well-known Wacker chemistry based on the Pd(II)–Cu(II) redox cycle. Copper is the major catalyst component by forming the CDC that interacts with phenols and CO to start the catalytic cycle. The metallic Pd as the active state for that reaction plays a secondary role by catalyzing the regeneration of organic oxidant like benzoquinone from hydroquinone. The role of Bu_4NBr has been known to activate phenols as a base. More importantly, however, it helps form and stabilize the active copper(I) complex $[Br^-–Cu(I)–Br^-]^-\cdots{}^+NBu_4$.

5. Conclusions

The nature and role of the active states of palladium and copper for the oxidative carbonylation of phenol and bisphenol-A were investigated through Pd and Cu *K*-edge XANES and EXAFS analyses. The initial state of Pd was carbon-supported metallic Pd with some fraction of oxidized surface. During the oxidative carbonylation, however, the metallic character of palladium was enhanced as shown by the XANES spectra and the particle size increased from 6.0 to 11.0 as determined by the quantitative EXAFS analyses of the Pd *K*-edge. The cuprous oxide as the initial state of copper was converted to a linear cuprous dibromide complex stabilized by tetrabutylammonium cation, which was elucidated from the qualitative XANES and EXAFS analyses at the Cu *K*-edge. Based on these results, a possible reaction scheme was proposed for the oxidative carbonylation of phenols employing the catalytic system of the Pd/C and the cuprous dibromide complex. Bu_4NBr was employed as a conventional base in order to activate phenols into phenoxides, but played an additional role of converting the crystalline Cu_2O into the active cuprous dibromide complex. The cuprous dibromide complex was found to be the active main catalytic component to produce the desired aromatic carbonates in the present system. The carbon-supported metallic Pd was responsible for the oxidative regeneration of hydroquinone to benzoquinone with coproduction of the sole by-product H_2O for the oxidative carbonylation of phenols.

Acknowledgments

This work was supported by LG Chem. Ltd. and the Korea Science and Engineering Foundation (KOSEF) through the Engineering Research Center (ERC). We appreciate the support of the Research Center for Energy Conversion and Storage. We also appreciate the support of Korean Ministry of Education and Human Resources Development through the BK 21 program.

References

[1] J.E. Hallgren, R.O. Mathews, J. Organomet. Chem. 175 (1979) 135.
[2] J.E. Hallgren, G.M. Lucas, R.O. Mathews, J. Organomet. Chem. 204 (1981) 135.
[3] J.E. Hallgren, G.M. Lucas, J. Organomet. Chem. 212 (1981) 135.
[4] M. Goyal, R. Nagahata, J. Sugiyama, M. Asai, M. Ueda, K. Takeuchi, J. Mol. Catal. A 137 (1999) 147.
[5] A. Vavasori, L. Toniolo, J. Mol. Catal. A 139 (1999) 109.

[6] H. Ishii, M. Goyal, M. Ueda, K. Takeuchi, M. Asai, Appl. Catal. A 201 (2000) 101.
[7] M. Takagi, H. Miyagi, T. Yoneyama, Y. Ohgomori, J. Mol. Catal. A 129 (1998) L1.
[8] H.Y. Song, E.D. Park, J.S. Lee, J. Mol. Catal. A 154 (2000) 243.
[9] H. Kezuka, F. Okuda, US patent 5336803, 1994.
[10] M. Mizukami, K. Hayashi, K. Iura, T. Kawaki, US patent 5380907, 1995.
[11] H. Iwane, H. Miyagi, S. Imada, S. Seo, T. Yoneyama, US patent 5543547, 1996.
[12] M. Takagi, K. Kujira, T. Yoneyama, Y. Ohgomori, US patent 5726340, 1998.
[13] M. Goyal, R. Nagahata, J. Sugiyama, M. Asai, M. Ueda, K. Takeuchi, Polymer 41 (2000) 2289.
[14] R.V. Chaudhari, A.A. Kelkar, S.P. Gupte, B.M. Ghanage, M.S. Qureshi, B. Moasser, E.J. Pressman, S. Sivaram, C.V. Avadhari, S. Kanagasabapathy, US patent 6222002, 2001.
[15] H. Ishii, M. Goyal, M. Ueda, K. Takeuchi, M. Asai, Macromol. Rapid Commun. 22 (2001) 376.
[16] W.B. Kim, J.S. Lee, Catal. Lett. 59 (1999) 83.
[17] W.B. Kim, J.S. Lee, J. Appl. Polym. Sci. 86 (2002) 937.
[18] W.B. Kim, K.H. Park, J.S. Lee, J. Mol. Catal. A 184 (2002) 39.
[19] W.B. Kim, E.D. Park, J.S. Lee, Appl. Catal. A 242 (2003) 335.
[20] M. Nomura, A. Koyama, KEK Rep. 89 (1989) 16.
[21] T. Ressler, J. Phys. IV 7 (1997) 269.
[22] E.A. Stern, M. Newville, B. Ravel, Y. Yacoby, D. Haskel, Phys. B 208/209 (1995) 117.
[23] J.J. Rehr, J.M. Leon, S.I. Zabinsky, R.C. Albers, J. Am. Chem. Soc. 113 (1991) 5135.
[24] A.F. Wells, Structural Inorganic Chemistry, 5th ed., Clarendon, Oxford, 1984.
[25] W.B. Kim, S.H. Choi, J.S. Lee, J. Phys. Chem. B 104 (2000) 8670.
[26] L.-S. Kau, D.J. S.-Solomon, J.E. P.-Hahn, K.O. Hodgson, E.I. Solomon, J. Am. Chem. Soc. 109 (1987) 6433.
[27] M. Matsuoka, W.-S. Ju, K. Takahashi, H. Yamashita, M. Anpo, J. Phys. Chem. B 104 (2000) 4911.
[28] J. Rothe, J. Hormes, H. Bonnemann, W. Brijoux, K. Siepen, J. Am. Chem. Soc. 120 (1998) 6019.
[29] F. Zhao, M. Shirai, Y. Ikushima, M. Arai, J. Mol. Catal. A 180 (2002) 211.
[30] G. Kiss, Chem. Rev. 101 (2001) 3435.
[31] D.P. Dissanayake, J.H. Lunsford, J. Catal. 206 (2002) 173.
[32] A. Rodriguez, C. Amiens, B. Chaudret, M.-J. Casanove, P. Lecante, J.S. Bradley, Chem. Mater. 8 (1996) 1978.
[33] A. Moen, D.G. Nicholson, M. Ronnig, J. Chem. Soc. Faraday Trans. 91 (1995) 3189.
[34] G. Lamble, A. Moen, G. Nicholson, J. Chem. Soc. Faraday Trans. 90 (1994) 2211.
[35] T.N. Sorrell, D.L. Jameson, J. Am. Chem. Soc. 105 (1983) 6013.
[36] R. Kumashiro, Y. Kuroda, M. Nagao, J. Phys. Chem. B 103 (1999) 89.
[37] B.K. Teo, EXAFS: Basic Principles and Data Analysis, Springer, Berlin, 1986.
[38] H. Grennberg, A. Gogoll, J.-E. Backvall, Organometallics 12 (1993) 1790.